Effects of Baroclinicity and Cooling on Frontal Subduction

YOSHIKAWA, Yutaka
Research Institute for Applied Mechanics, Kyushu University

AKITOMO, Kazunori
Graduate School of Science, Kyoto University

YOON, Jong-Hwan
Research Institute for Applied Mechanics, Kyushu University

https://doi.org/10.15017/6768396

出版情報：九州大学応用力学研究所所報. 120, pp.41-46, 2001-02. Research Institute for Applied Mechanics, Kyushu University
バージョン：
権利関係：

Effects of Baroclinicity and Cooling on Frontal Subduction

Yutaka YOSHIKAWA *1, Kazunori AKITOMO *2, and Jong-Hwan YOON*1

E-mail of corresponding author: *yosikawa@riam.kyushu-u.ac.jp*

(Received November 30, 2000)

Abstract

The authors examined the effect of oceanic baroclinicity and atmospheric cooling on the subduction in baroclinic ocean using three dimensional nonhydrostatic model. It turns out that stronger baroclinicity causes larger subduction rate despite similar penetration speed of the depth to which subducted water is transported (subduction depth), while stronger cooling results in more rapid penetration speed of the subduction depth though it affects little on the subduction rate as long as cooling is imposed. These results suggests that both baroclinicity and cooling are important parameters for heat and material transports between the surface mixed layer and the interior baroclinic ocean and hence for decadal variations in climate systems.

Key words : *Baroclinic Instability, Convection, Combined Effect, Subduction*

1. Introduction

Subduction is the transfer of the mixed layer water into the stratified interior ocean and is a key process for heat and material transports in intermediate and deep layers [e.g.,Woods[1)]]. Several studies have been made to understand the dynamics involved in subduction process so far. In the region of intense baroclinicity, such as in the subtropical and subpolar frontal zones where subduction is suggested to be an essential ingredient of decadal variabilities in climate systems [e.g., Hanawa[2)]], baroclinic instability and following frontogenetic process play a central role in subduction [Pollard and Regeir[3)]; Spall[4)]]. Subduction in such frontal regions is then called frontal subduction. Recently, prompted by the fact that subduction into intermediate and deep layers mainly takes place in winter [Iserin[5)]], the dynamics of frontal subduction under the atmospheric cooling was investigated by Yoshikawa *et al.*[6)]. They found that combined effect of baroclinic instability and convection is so significant that convection acts not only to mix water vertically but also to intensify frontogenetic process. As a result, frontal subduction is enhanced by atmospheric cooling to a large degree.

It is then suggested that frontal subduction varies in its intensity with both atmospheric cooling and oceanic baroclinicity. However, little attention has been given to this point so far. In order for further understanding of frontal subduction and its possible roles in decadal climate variabilities, the response of frontal subduction to the variations in baroclinicity and cooling needs to be clarified. The present study is then intended to investigate and quantify the effects of baroclinicity and cooling on frontal subduction. To this end, numerical experiments are performed using a nonhydrostatic model.

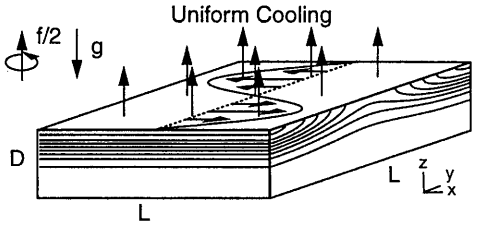

Figure 1 Schematic view of the model configuration. Contours drawn on the sides and solid line on the top schematically represent density structure and the geostrophic velocity profile, respectively.

2. Numerical Model

The model used in this study is the same as used in Yoshikawa et al.[6)], in which a simple rectangular ocean ($L(50\ \mathrm{km}) \times L \times D(1\ \mathrm{km})$) on an f- plane ($f = 10^{-4}\ \mathrm{s}^{-1}$) is considered (Fig. 1). Initial density structure $\rho(y, z)$ is assumed to be taken as

$$\rho(y,z) = -\left(\rho_m \cos\left(\frac{2\pi y}{L}\right) + \rho_v\right) \exp\left(-\frac{z^2}{h^2}\right) + \rho_b. \quad (1)$$

*1 Research Institute for Applied Mechanics, Kyushu University
*2 Graduate School of Science, Kyoto University

Table 1 Parameters used in each experiment.

		REF	WBR	SBR	WCL	SCL
ρ_m	(10^{-2} kg m^{-3})	5	2.5	10.	5.	5.
D_f	(10^{-6} kg m^{-2} s^{-1})	6.4	6.4	6.4	3.2	12.8

Here, ρ_m is the meridional density difference between the central latitude ($y = L/2$) and the southern/northern ends ($y = 0, L$) which determines the intensity of baroclinicity, $\rho_v(10.5 \times 10^{-2}$ kg m$^{-3})$ is vertical density difference between the surface and the bottom ($z = -D$), $\rho_b(1027.35$ kg m$^{-3})$ is density at the bottom, and $h(300$ m) is the vertical decay scale. Initial velocity structure is assumed to be geostrophic current balancing with this density structure with reference level being at the bottom. At the surface, uniform density flux D_f is imposed. Both the surface and bottom boundaries are assumed to be rigid and smooth, while side boundaries are assumed to be periodic.

Governing equations are momentum equations, continuity equation and advective-diffusive equation for water density under Boussinesq and incompressible approximations:

$$\frac{\partial \mathbf{u}}{\partial t} + (\mathbf{u}\cdot\nabla)\mathbf{u} + f\hat{\mathbf{z}}\times\mathbf{u} = -\frac{1}{\rho_0}\nabla p - \frac{\rho}{\rho_0}g\hat{\mathbf{z}} + \nu_h\nabla_h^2\mathbf{u} + \nu_z\frac{\partial^2\mathbf{u}}{\partial z^2}, \quad (2)$$

$$\nabla\cdot\mathbf{u} = 0, \quad (3)$$

$$\frac{\partial \rho}{\partial t} + \mathbf{u}\cdot\nabla\rho = \kappa_h\nabla_h^2\rho + \kappa_z\frac{\partial^2\rho}{\partial z^2}, \quad (4)$$

where $\mathbf{u}$ is the velocity vector, $\rho_0(= 1027$ kg m$^{-3})$ is reference density, $g(= 9.8$ m s$^{-2})$ is the acceleration due to gravity, p is the pressure, $\hat{\mathbf{z}} = (0, 0, 1)$ is a unit vector in the z direction. Eddy viscosities (ν_h, ν_z) and eddy diffusivities (κ_h, κ_z) are assumed to be constant ($\nu_h = \kappa_h = 5$ m^2 s^{-1}, and $\nu_z = \kappa_z = 2 \times 10^{-2}$ m^2 s^{-1}). Distribution of dynamically passive tracer (C) is also calculated using Eq.(4). Its concentration is initially set to zero in the whole domain and held at unity at the surface during the integration. Thus, high tracer concentration corresponds to newly ventilated (aerated) water. Other boundary conditions for tracer concentration are the same for water density. Small grid size ($\Delta x = \Delta y = 195$ m, $\Delta z = 33$ m) and short time interval ($\Delta t = 135$ s) are chosen so as to resolve convective plumes of 1 km horizontal scale.

In the reference experiment (hereafter called REF), ρ_m and D_f are set to be 5×10^{-2} kg m^{-3} and 6.4×10^{-6} kg m^{-2} s^{-1}, respectively. These values are the same as used in Yoshikawa et al.[6] and do not differ so much from the observed climate values in the actual frontal regions. For clear understanding of the effects of baroclinicity and cooling on frontal subduction, additional four experiments are carried out (Table 1). To see the effect of baroclinicity, ρ_m is set to half (WBR) and double (SBR) of that used in REF while D_f is unchanged. To see the effect of cooling, D_f is set to half (WCL) and double (SCL) of that used in REF while ρ_m is unchanged. Note that larger (smaller) ρ_m also corresponds to relatively weaker (stronger) stratification in the central region (12.5 km $< y <$ 37.5 km) and relatively stronger (weaker) stratification in the outer regions ($y <$ 12.5 km, 37.5 km $< y$) (Eq.(1)), so that intensity of convection will be changed due to the different values of ρ_m even though the same D_f is used.

3. Results

Qualitatively similar time evolutions of convection and baroclinic instability are observed in all experiments. Convection first develops from the most weakly stratified area ($y \simeq 25$ km) and forms mixed layer in the upper layer. Thereafter, linear baroclinic instability develops in the region of strong baroclinicity (5 km $\leq y \leq$ 20 km, 30 km $\leq y \leq$ 45 km; called the baroclinic region). Baroclinic instability develops into finite amplitude within 5 $\sim$ 10 days of the onset time of convection, and finite baroclinic instability causes strong restratification in the upper layer and reduces convective activity there. At the same time, finite baroclinic instability induces frontogenetic process to generate the downdraft along density front which is greatly enhanced by cooling (convection). Figure 2 shows the horizontal sections of density and downward velocity at the time when strongest frontal downdraft is observed. The strong frontal downdrafts are generated associated with bent-back density front in the outer regions of the baroclinic region. Figure 3 shows the vertical sections of two-dimensional velocity vector, density, and tracer concentration. It is clearly found that strong frontal downdraft transports surface ventilated water into greater depths along isopycnal surfaces. Figure 4 shows horizontal sections of horizontal velocity vector and tracer concentration. Patches of ventilated water, characterized by anomalously weak stratification (not shown) and anticyclonic circulation, are found to be formed in deeper layer associated with the strong frontal downdrafts (Fig. 2). Horizontal scale of the ventilated patch is closely related to the wavelength of finite baroclinic

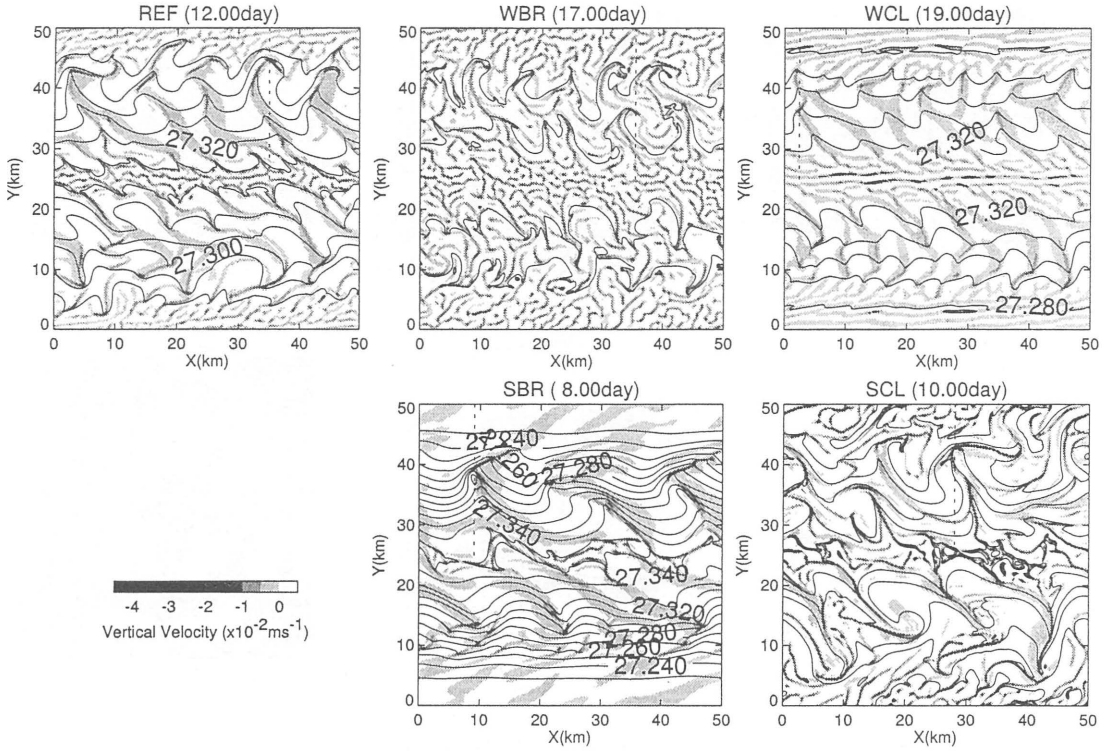

Figure 2 Horizontal sections ($z = -100$ m) of vertical velocity (shaded regions) and density (solid lines). Contour interval is 1×10^{-2} kg m^{-3}. Dotted line denotes the longitude of vertical section shown in Figure 3.

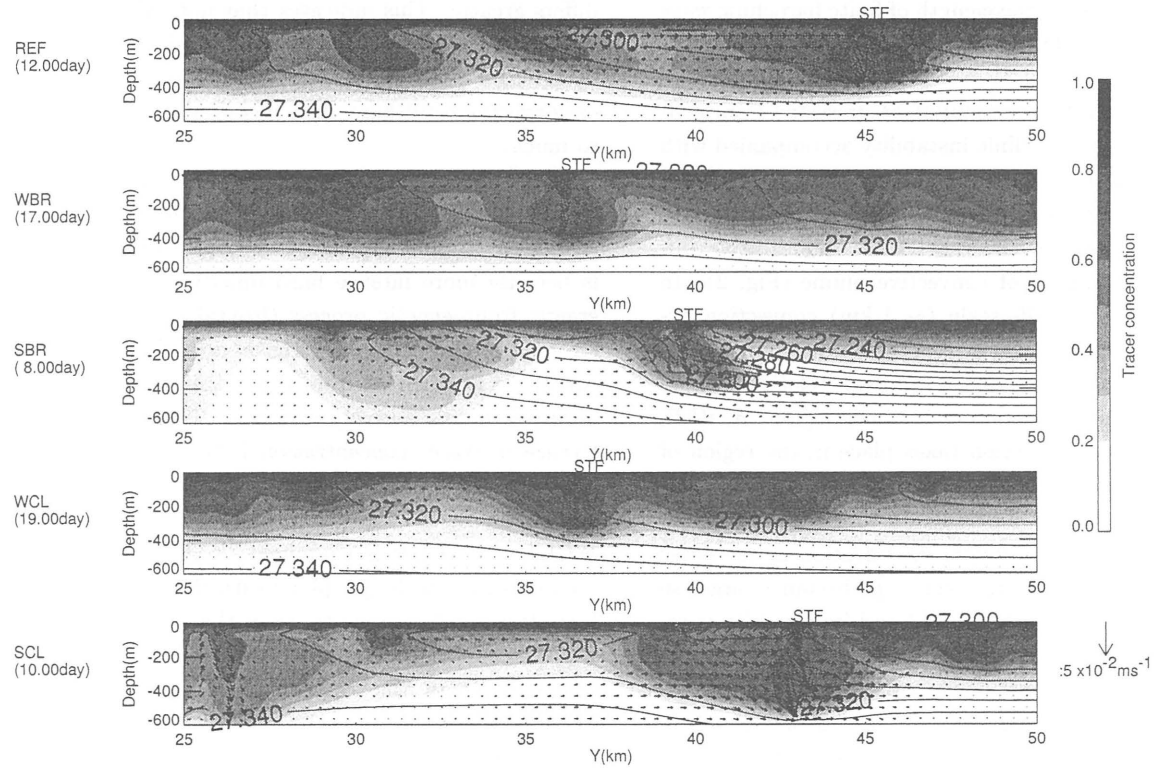

Fig. 3 Meridional sections of density (solid lines), tracer concentration (shaded regions), and two-dimensional (y-z) velocity vector (arrows). Contour interval is 1×10^{-2} kg m^{-3}. STF denotes the strong frontal downdraft.

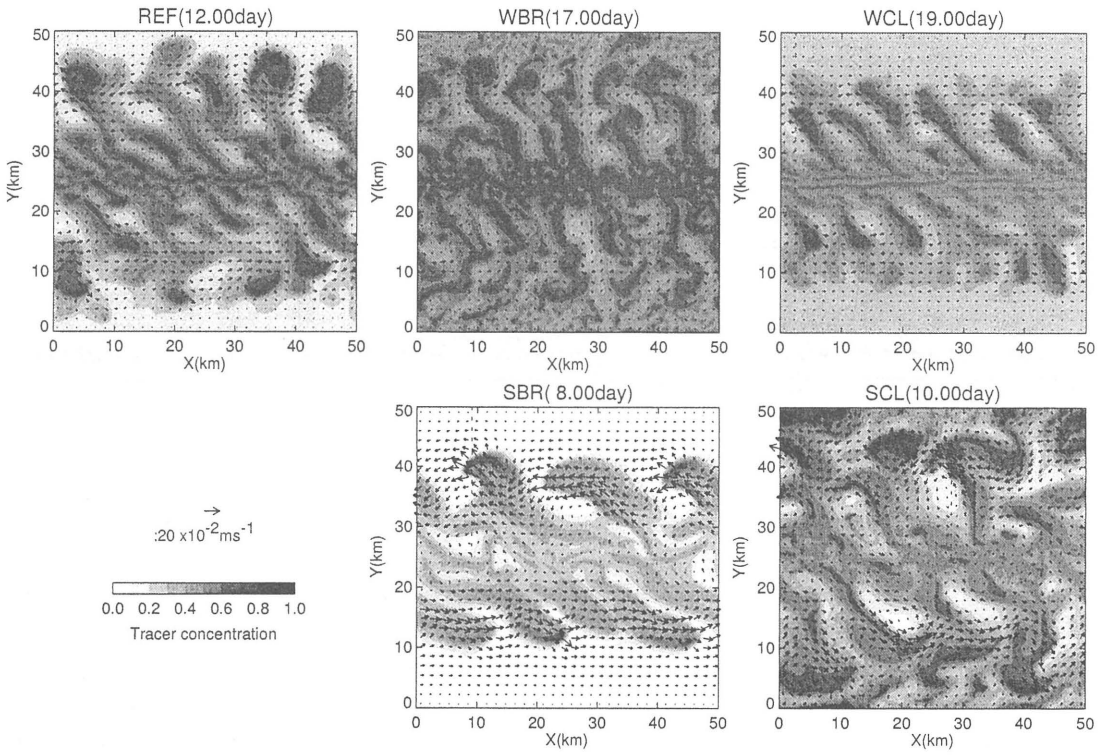

Fig. 4 Horizontal sections ($z = -300$ m) of tracer concentration (shaded areas) and horizontal velocity vector (arrows).

wave (Figs. 2 and 4). As the restratification in the upper layer progresses, wavelength of finite baroclinic wave and horizontal scale of ventilated patch increase accordingly.

Although similar sequential progressions from convection to finite baroclinic instability accompanied with strong frontal downdraft are commonly observed in the above experiments, some quantitative differences are also found. One of the remarkable quantitative differences is a number of convective plume (Fig. 2). In WBR, a lot of small- scale ($\sim$ 1 km) convection occurs in the region of 0 km $\leq y \leq$ 5 km, 20 km $\leq y \leq$ 30 km, 45 km $\leq y \leq$ 50 km, while a relatively small number of convection occurs in those regions in REF, and only a few convection takes place in the region of 23 km $\leq y \leq$ 27 km in SBR. Main reason for this difference stems from the difference in initial stratification. As ρ_m becomes large, initial stratification in the outer regions ($y \leq$ 12.5 km, 37.5 km $\leq y$) becomes large, so that convection onset is delayed and its intensity is reduced there. The other reason is the restratification due to finite baroclinic instability. Large ρ_m corresponds to intense baroclinic instability which causes strong restratification in the upper layer. As a result, the area of convection near the central latitude ($y \simeq L/2$) is reduced. Between WCL, REF, and SCL, on the other hand, the number of convective plumes does not differ significantly, though its intensity (e.g., vertical velocity) differs greatly. This indicates that not only convection but also baroclinic instability are intensified (weakened) by stronger (weaker) cooling, so that relative intensity of convection and baroclinic instability does not differ so much.

The other remarkable difference is found in the intensity of the strong frontal downdraft. It becomes strong as ρ_m and D_f becomes large (Table 2). This is because more intense baroclinicity causes more energetic frontogenetic process (frontal downdraft) while stronger cooling intensifies frontal downdraft to a larger extent. It is expected from this result that subduction increases as ρ_m and D_f increase. Therefore, the difference in tracer concentration between the above experiments (REF, WBR, SBR, WCL, and SCL) and the corresponding 2D experiments (REF2, WBR2, SBR2, WCL2, and SCL2) is examined. The 2D experiments are performed in the y-z plane with the same initial and boundary conditions as those in the corresponding 3D experiments. Since no baroclinic instability develops in 2D experiments, the tracer difference between 3D and 2D experiments is owing to baroclinic instability, e.g., subduction process.

Figure 5 shows time evolutions of horizontally averaged tracer difference between 3D and 2D experiments in the baroclinic region (where subduction mainly takes

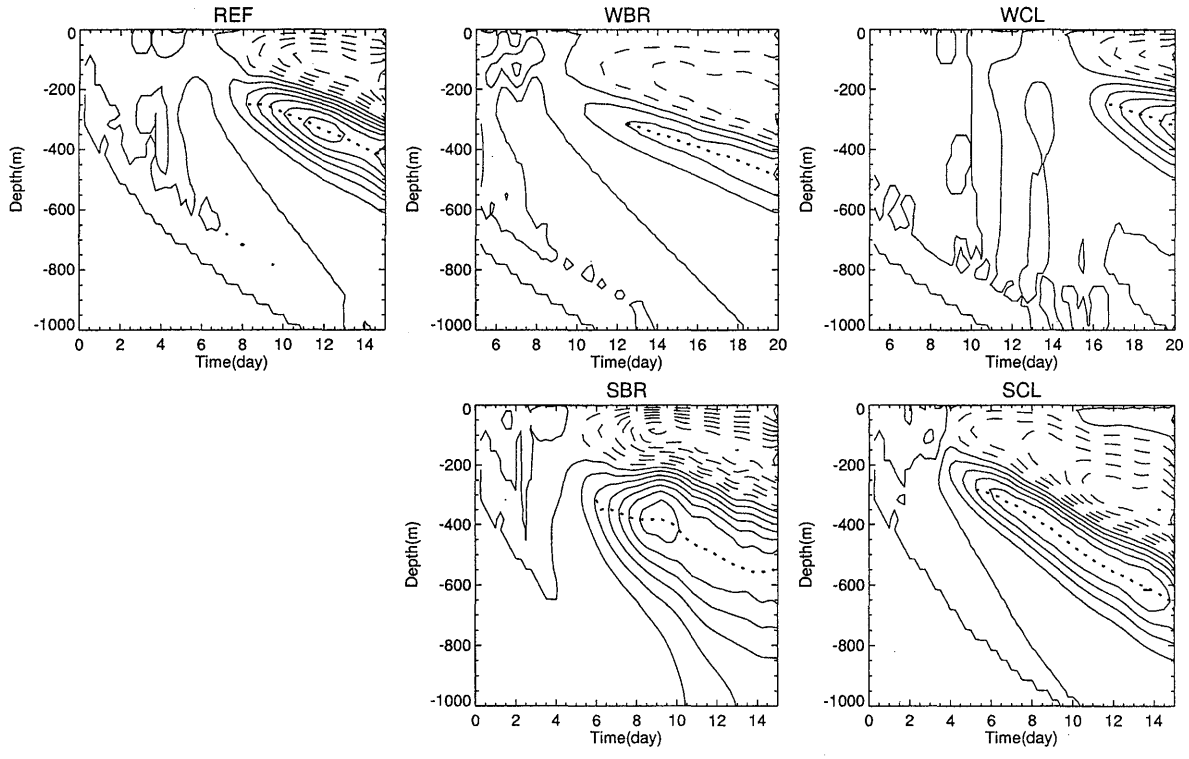

Fig. 5 Difference of horizontally averaged tracer concentration ΔC between 3D and 2D experiments as a function of time (abscissa) and depth (ordinate). Contour interval is 1×10^{-2}. Solid lines represent positive value, while dashed lines represent negative one. Dotted line represents the characteristic depth of subduction.

place):

$$\Delta C = \overline{\overline{C_{3D}}^{br}}^{x} - \overline{\overline{C_{2D}}^{br}}. \qquad (5)$$

In the above,

$$\overline{(\,)}^{x} = \frac{1}{50\ \mathrm{km}} \int_{0\ \mathrm{km}}^{50\ \mathrm{km}} dx,$$

$$\overline{(\,)}^{br} = \frac{1}{30\ \mathrm{km}} \left[\int_{5\ \mathrm{km}}^{20\ \mathrm{km}} dy + \int_{30\ \mathrm{km}}^{45\ \mathrm{km}} dy \right].$$

In Fig. 5, solid lines represent positive values while dashed lines represent negative values. Overall feature is that ΔC is negative in upper layer and positive in deeper layer. The region of negative ΔC approximately corresponds to the mixed layer from which ventilated water (high tracer concentration) is transported. It is clear from Fig. 5 that subduction process transports surface ventilated water in the mixed layer into greater depths in all experiments. The difference in the onset time of subduction is owing to the difference in the onset time of convection which acts as an initiator of baroclinic instability (Yoshikawa *et al.*[6]). The differences in the onset times between the experiments may be unrealistically larger than actual, since artificially large vertical diffusivity is used in the present experiments which diffuses unstable stratification near the surface more rapidly and delays convection onset for a longer time than actual. It seems rather interesting that the speed of downward penetration of the layer of positive ΔC seems to differ between the experiments. The characteristic depth of subduction can be defined as the depth of largest ΔC, which is plotted by dotted line in Fig. 5. It is found that the speed of downward penetration of the subduction depth changes greatly between WCL, REF, and SCL, while it changes little between WBR, REF, and SBR (Table 2). This is probably because large (small) D_f causes rapid (slow) deepening of the horizontally averaged mixed layer so that the subduction depth rapidly (slowly) deepens accordingly, while the change in ρ_m affects little on the deepening of horizontally averaged mixed layer so that characteristic depth of subduction does not differ between WBR, REF, and SBR.

The net amount in subduction *Sub* can be evaluated by calculating total tracer difference below the mixed layer base (MLB):

$$Sub = \overline{\int_{-D}^{MLB(y)} (\overline{C_{3D}}^{x} - C_{2D}) dz}^{br}. \qquad (6)$$

In the above, the mixed layer base is defined as the boundary between the negative ΔC in upper layer and positive ΔC in deeper layer. Figure 6 shows time evolutions of *Sub*. After 2~5 days from the onset of subduction, *Sub* increases almost linearly with time. Notewor-

Table 2 Maximum downward velocity w_{max}, penetration rate, and subduction rate in each experiment.

		REF	WBR	SBR	WCL	SCL
w_{max}	$(10^{-2}$ m $s^{-1})$	-4.4	-3.9	-6.2	-2.5	-9.4
Penetration Rate	(m day^{-1})	-22.2	-24.7	-25.9	-20.5	-41.0
Subduction Rate	$(10^{-4}$ $s^{-1})$	2.71	0.75	5.76	2.81	2.64

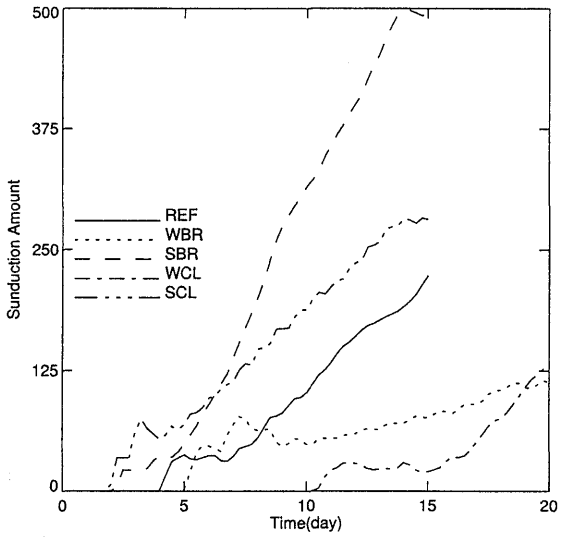

Fig. 6 Time evolutions of *Sub*.

thy is that during the linear growth of *Sub*, the subduction rate (time change of *Sub*) differs greatly in WBR, REF, and SBR, while it is almost the same in WCL, REF, and SCL (Table 2). This is explained as follows. As ρ_m increases, frontal downdraft is intensified greatly while horizontally averaged convective activity is not enhanced (Fig. 2). As a result, subduction rate becomes large according to the intensification of frontal downdraft due to increasing ρ_m. On the other hand, as D_f increases, both frontal downdraft and convection are equally intensified. This is easily understood from the fact that the relative intensity of convection and baroclinic instability does not differ greatly between WCL, REF, and SCL, as discussed before (Fig. 2). Therefore, although the large amount of ventilated water is transported from the mixed layer by intensified strong frontal downdraft, it is likely to be re-entrained into the rapidly deepening mixed layer. As a result, subduction rate does not vary greatly with D_f.

4. Summary and discussion

We investigated the effect of baroclinicity and cooling on frontal subduction. It is clearly found that stronger baroclinicity causes larger subduction rate despite similar penetration speed of the subduction depth, while stronger cooling results in more rapid penetration speed of the subduction depth though it affects little on subduction rate as long as cooling is imposed.

These results clearly demonstrate that both baroclinicity and cooling are important parameters for heat and material transports between the surface mixed layer and the interior ocean and hence for decadal climate variations. However, recent climate studies give attention primary to the variation of atmospheric cooling when annual variations of subduction is discussed. We propose that much attention should be also given to the variations in baroclinicity as well as cooling.

Acknowledgments

The authors express sincere thanks to Prof. Awaji in Kyoto University for his instructive discussions. Part of this study was supported by a Grant-in-Aid for Scientific Research, number 3265, from the Ministry of Education, Science, Culture, Japan.

References

1) Woods, J.D.: The physics of thermocline ventilation, in *Coupled Ocean-Atmosphere Models,* edited by J.C.J. Nihoul, pp. 543-590, Elsevier Sci., New York, 1985

2) Hanawa, K.: Decadal- and interdecadal-scale variabilities in the North Pacific, *Kaiyo Monthly*, Vol.29, (1997) 637-641 (in Japanese)

3) Pollard, R.T., and L.A. Regier: Vorticity and vertical circulation at an ocean front, *J. Phys. Oceanogr.*, Vol.22, (1992) 609-625, 1992

4) Spall, M.A.: Frontogenesis, subduction, and cross-front exchange at upper ocean fronts, *J. Geophys. Res.*, Vol.100, (1995) 2543-2557

5) Iserin, C. O. D.: The influence of vertical and lateral turbulence on the characteristics of waters at mid-depths, *Trans. Amer. Geophys. Union*, Vol.20, (1939) 414-417

6) Yoshikawa, Y., K. Akitomo, and T. Awaji: Formation Process of Intermediate Water in Baroclinic Current under Cooling, *J. Geophys. Res.*, in press